



AIAA-2003-1017

**Structure of Hydrogen- and
Methane- Fueled Partially
Premixed Planar and Tubular
Flames**

J. Wehrmeyer, Z. Cheng, P. Wang,
D. Mosbacher and R. Pitz
Vanderbilt University, Nashville, TN

41st Aerospace Sciences Meeting & Exhibit

6-9 January 2003

Reno, Nevada

For permission to copy or to republish, contact the copyright owner named on the first page.

**For AIAA-held copyright, write to AIAA Permissions Department,
1801 Alexander Bell Drive, Suite 500, Reston, VA, 20191-4344.**

STRUCTURE OF HYDROGEN- AND METHANE-FUELED PARTIALLY-PREMIXED PLANAR AND TUBULAR FLAMES

Joseph A. Wehrmeyer,* Zhongxian Cheng,† Peiyong Wang,‡ David M. Mosbacher,§ Robert W. Pitz¶
Mechanical Engineering Department, Vanderbilt University, Nashville, TN 37235

Abstract

To understand the influence of flame curvature on the structure of premixed flames, and to understand the interaction between hot products and lean limit reactant mixtures, tubular and planar premixed flames are examined both experimentally and numerically. Using visible Raman spectroscopy, the structure of lean hydrogen-air flames is probed in either an optically-accessible tubular burner or a standard opposed jet burner. Good agreement between experimental and numerical profiles is found for both types of burners at low stretch rates, but at high stretch values there is marked disagreement between experimental and numerical data for the tubular premixed flames. Experimental extinction stretch rates are much lower than numerically predicted, for both types of hydrogen-air flames. However for methane-air tubular premixed flames there is good agreement between experimental and numerical extinction stretch rates for a wide range of lean equivalence ratios. For one particular methane-air equivalence ratio (0.53) the numerically-predicted peak temperatures for either tubular or planar premixed flames are generally the same across a wide range of stretch rates, showing curvature has little influence for these types of near-unity Lewis number flames. Planar partially-premixed flames produced by a lean methane-air jet ($\phi = 0.69$ or 0.56) opposed by a lean hydrogen-air jet ($\phi=0.28$) were examined experimentally and numerically. Excellent agreement among experimental and numerical data was obtained for both methane-air equivalence ratios, and the lower one showed evidence of a “negative flame speed” flame where combustion occurs only via the diffusion of methane across the stagnation plane into the hot products jet.

Introduction

Lean premixed combustion provides clean and efficient burning in practical devices, such as direct injection spark ignition engines for ground transportation, and lean-burn gas turbine engines for

power generation. Lean premixed flames in these devices are turbulent and unsteady. To understand the effect of high strain rate (flame stretch) in these devices, planar opposed jet premixed flames have been studied under both steady and unsteady conditions.

However, the premixed flame surfaces typically found in practical devices are curved. It is well known that stretch and curvature in the presence of unequal rates of heat and mass diffusion (nonunity Lewis number) can lead to substantial changes in the flame structure (i.e., gas composition, temperature) and flame extinction.^{1,2} For example, curved “tubular” flames of methane-air can exist at conditions that are well below the lean flammability limit.³ Such flames have the promise of lowering pollutant emissions from nitric oxides to even lower levels. This is the motivation for the work described in this paper, which investigates the structure of lean premixed flames under the influence of stretch and flame curvature. Methane-air flames are examined, but also hydrogen-air flames are examined since their chemistry is better known than methane-air combustion chemistry.

A convenient burner for the study of the simultaneous effect of stretch and curvature is the tubular flame burner. A tubular premixed flame produced in this kind of burner is sketched in Fig. 1. In the tubular flame the premixed reactants flow radially inward to form an axisymmetric flame tube. The exhaust gases from the tubular flame flow axially out the ends of the tube. This configuration is attractive for numerical study as the two-dimensional flowfield can be reduced to a two-point boundary value problem along a radius in the stagnation plane. The flame structure can then be determined in a short time, even when using a complex chemical mechanism coupled with detailed molecular transport, and even including radiation heat transfer.

The tubular flame has been modeled by a number of workers in order to predict flame structure and extinction as functions of the inlet velocity boundary condition. Numerical models of detailed transport and full or reduced chemistry have been reported by Smooke and Giovangigli,⁴ Nishioka et al.,⁵ Ju et al.,³ and Yamamoto et al.⁶ In addition, high-energy asymptotics using 1-step chemistry have been used to study tubular flame structure and extinction.⁷⁻⁹

There have been a number of experimental studies of tubular burners that have been reviewed by

* Research Associate Prof., Senior Member, AIAA

† Graduate Student, Student Member, AIAA

‡ Graduate Student

§ Graduate Student

¶ Prof. and Department Chair, Associate Fellow, AIAA

Ishizuka,¹⁰ Using a rotating flow burner similar to Ishizuka,¹¹ Yamamoto et al.¹² have experimentally investigated tubular premixed flames created in a low stretch vortex. Ishizuka¹³ and Ogawa et al.¹⁴ injected premixed reactants radially inward through the walls of an open porous cylindrical tube to examine curvature effects at low rates of stretch. Using a burner that directed premixed reactants radially inward completely around the flame circumference, Kobayashi and Kitano^{15,16} examined the extinction characteristics of propane-air and methane-air premixed tubular flames at high rates of stretch and compared them to similar opposed jet flames. In these experiments, almost all the flame measurements are made with intrusive probes. Temperature is determined by thermocouples and composition measured by sampling microprobes.¹⁰

The major deficiency of the previous tubular burner studies is the lack of non-intrusive measurements of the flame structure (i.e., temperature and chemical composition) needed for comparison to the detailed numerical predictions of tubular flames. Previously-studied tubular burners had limited optical access through the burned gas exit ports. The only non-intrusive measurements are laser Doppler velocimetry measurements by Kobayashi and Kitano¹⁶ and OH laser-induced fluorescence by Yamamoto et al.¹² In the present work an optically accessible cylindrical burner is used that allows probing of the tubular premixed flames using visible Raman scattering.

Experimental

Figure 2 shows the tubular burner used for this research. It consists of a central radial nozzle flanked by co-flow radial nozzles that dilute the unburnt reactants to keep unstretched combustion, outside of the burner, to a minimum. The diameter of the radial nozzle is 30 mm, and its width is 20 mm. It is similar to the cylindrical burner of Kobayashi and Kitano¹⁵ but has the addition of optical access ports for laser diagnostics. These ports are at three locations around the cylindrical burner. Two of the three ports allow a laser to enter and exit the burner. A third optical port, located at right angles to the two laser ports, provides a view to the light detection system used to collect Raman or fluorescence signals. For this work a characteristic stretch rate (κ) for this tubular burner is defined as $4V/D$, where V is the reactant mixture velocity (in cm/sec) at the nozzle exit and D is the nozzle diameter (3 cm). This definition of κ is consistent with the work of others.^{15,16}

The opposed jet burner used for this work is a modification of the design by Seshadri et al.¹⁷ It consists of two 25 mm diameter straight jets, which are separated by 12.5 mm. The nozzle exits, which normally hold a series of wire screens,¹⁷ are modified for this work by replacing the screens with honeycomb

metal inserts to prevent premixed flame anchoring at the nozzle exits. If the momenta of the two flows are balanced, a stagnation plane exists halfway between the two jets. For the bottom jet, co-flow nitrogen shields the flame and prevents outside air from mixing with the jet. The hot exhaust gas is sucked into an annular exhaust section around the top jet. The top jet and annular exhaust are cooled by a water jacket system. For this work the characteristic stretch rate κ for the opposed jet burner is defined as:

$$\kappa = (2V_1/L)(1+(\rho_1 V_1^2/\rho_2 V_2^2)^{1/2}) \quad (1)$$

where L is the nozzle separation length, and V_i and ρ_i are the exit velocity and density for nozzle i and the subscripts 1 and 2 refer to arbitrary choices of the opposed jet nozzles. When the momenta of the two jets are equal Eq. 1 reduces to $4V_1/L$. This definition of κ is a typical one used for opposed jet flows.¹⁸

A schematic of the visible Raman system is shown in Fig. 3. Visible laser Raman spectroscopy is used to measure temperature and species concentrations through the flame. The Raman signals are created by a frequency-doubled, pulsed (10 Hz) Nd-YAG (532 nm) laser. The laser output is focused to a beam waist of ~ 0.25 mm to improve spatial resolution transverse to the laser beam. Energy output of the laser is limited to ~ 225 mJ/pulse due to losses from a mirrors-beamsplitter arrangement, which is used to prevent laser-induced breakdown at the laser focus by stretching the effective pulse length from 7 ns to ~ 35 ns.

The Raman scattered light is collected at 90° to the laser beam using a 75 mm diameter F/2 achromat lens and relayed by another lens into a modified single grating spectrograph.¹⁹ The light detector is a cryogenically cooled, back-illuminated CCD array (1024 x 1024 pixels), allowing one-dimensional spatially resolved, time-averaged measurements of Raman signals from all major species. The measured spatial resolution of the imaging system is ~ 120 μm along the 4.6 mm imaged length of the laser.

A 2.5 mm thick OG-550 colored-glass filter and an infrared filter are mounted in series at the entrance slit to minimize the amount of 532 nm light and stray infrared light entering the spectrograph. To efficiently gate the camera and reduce time-continuous background flame luminosity, a 44 μs ferroelectric liquid crystal (FLC) is used in series with a 6 ms mechanical shutter at the spectrometer entrance slit, with both open only during the laser pulse. A total of 600 single-pulse Raman images are averaged on the CCD. For the Raman measurements, the laser beam passes through the diameter of the flame tube at the zero axial position (the axial-plane of the stagnation

point). Based on the spatial resolution of the system, each integrated linewise image provides ~38 useable measurement points. Given the sampling length of the imaging system, the tubular burner is translated once in the zero axial-plane; thus, allowing the flame structure along the entire diameter of the flame tube to be recorded.

For data in the opposed jet flame, the 4.6 mm image laser length is completely binned into one superpixel to obtain only one high signal strength spectrum at each axial location along the burner axis. The opposed jet burner is translated axially with respect to the Raman system to obtain measurement profiles.

The experimental measurements of temperature and major species concentrations are derived from the Raman signals through an experimental calibration of the Raman system, using several calibration flames produced in a “Hencken” multi-element flat-flame diffusion burner. The ideal gas law is used to relate measured total number density to temperature assuming atmospheric pressure. For calibration conditions, fuel and air flowrates were measured with mass flow meters with accuracies of $\pm 1\%$ of their full scale. The accuracy of the temperature measurements, $\pm 2.5\%$, was evaluated by comparing experimental Raman temperature measurements from H₂-air calibration flames with adiabatic flame temperatures based on measured reactant flowrates.

In order to numerically model premixed tubular flames, the Oppdif²⁰ program was modified to account for the radial geometry. Oppdif normally models opposed jet flames of axial symmetry, where the reactants originate along the symmetry axis and exit radially away from the axis. Flame structure is then mapped onto the axial dimension. In a tubular flame, the radial coordinate, instead of the axial coordinate, is used as the spatial dimension through which flame structure is mapped. By transforming the spatial coordinate and seeking a similarity solution of the two-dimensional conservation equations, the tubular flame can be modeled as a two-point boundary value problem. The Oppdif program was modified for the tubular flame geometry, and the resulting set of differential equations for the tubular flame are given in Ref. 4.

Hydrogen-Air Tubular and Planar Flames

Several lean hydrogen-air flames have been investigated using the Vanderbilt tubular burner coupled to the visible Raman system.²¹ In that work it was found that there was excellent agreement between experiment and simulations at low stretch ($\kappa < 127 \text{ sec}^{-1}$), using a recently-developed hydrogen-air chemistry mechanism.²² Figure 4 shows one set of results from that investigation, where a hydrogen-air premixed

flame with an equivalence ratio (ϕ) of 0.175 is subjected to a stretch rate of 190 sec^{-1} . The measured peak temperature of this flame is significantly lower than the numerically-predicted temperatures provided by several hydrogen-air mechanisms, all of which are described in Ref 21. The mechanism providing the strongest flame with the highest peak temperature is that of Mueller et al.²² and its predictions are also displayed on Fig. 4 along with the Raman measurements. There is approximately a 200 K difference between the experimentally-measured peak temperature and the predicted peak temperature provided by the Mueller et al. mechanism.

In an effort to determine the reason for the difference between the two peak temperatures for the flame of Fig. 4, the rate of molecular diffusion for H₂ was increased and then decreased from its standard value. In addition thermal diffusion was “turned on” and “off” to determine its influence. While changing the H₂ molecular diffusion rate and/or changing thermal diffusion significantly changes the modeled temperature profiles, neither modification depresses the numerical temperature profile to a low enough level to match the experimental profile, as shown in Figure 5.

Flat opposed jet flames of lean hydrogen-air ($\phi=0.175$) have also been examined to see if similar discrepancies exist between numerical and experimental temperature profiles as in the tubular flames at 190 sec^{-1} . Figure 6 shows the experimental and numerical results for a flame with a 183 sec^{-1} stretch rate. There is excellent agreement between the numerical and experimental profiles of temperature and major species mole fractions for this planar flame, which is very near extinction. The experimental extinction stretch rate for this flat flame is just slightly above 183 sec^{-1} . Interestingly, the numerically predicted extinction stretch rate for the $\phi=0.175$ planar hydrogen-air flame is approximately 290 sec^{-1} , significantly above what can be achieved in the lab. Thus Fig. 6 shows data for the highest stretch rate that can be experimentally realized for this particular equivalence ratio, and shows good agreement among experimental and numerical data for this high stretch rate situation, in contrast to the tubular flame where considerable discrepancy existed between the experimental and numerical data sets at $\kappa=190 \text{ sec}^{-1}$.

Figure 7 shows peak temperature versus stretch rate for tubular and planar hydrogen-air premixed flames with an equivalence ratio of 0.175. Both experimental values and numerically-predicted values are shown. Also shown in Fig. 7 is the value for the adiabatic equilibrium flame temperature (875 K) for these flames, and shows that even for the planar flames there is significant stretch-induced increase of flame temperatures. The numerically-predicted peak temperatures for the tubular flame change only slightly

with increasing stretch rate, dropping only from a high of 1370 K down to 1280 K at an extinction stretch rate of approximately 780 sec^{-1} (not shown). However the experimentally-measured peak temperatures drop from a high of 1330 K down to 1100 K before extinction is encountered at $\kappa = 220 \text{ sec}^{-1}$. Thus for both the planar and tubular flames there is the similar trend of the experimental extinction stretch rate being significantly lower than the numerically-predicted value.

Methane-Air Tubular and Planar Flames

Several methane-air tubular and planar premixed flames are also examined, although for this work no Raman-derived data are presented. Using the same tubular burner as for the hydrogen-air flames, the extinction stretch rate for lean methane-air flames is determined. This experimental data is shown in Fig. 8, along with numerically predicted extinction stretch rates using two different reaction mechanisms.^{23,24} For the methane-air data, in contrast to the hydrogen-air results, the agreement is good between the experimental and numerical data sets. In other words the experimentally measured extinction stretch rate is similar to the numerically predicted extinction stretch rate, and this is true for a wide range of equivalence ratios. In addition, it makes little difference which of the two reaction mechanisms is used. The flowmeter used to measure methane flowrate, which determines flame equivalence ratio, is currently undergoing a calibration evaluation and the uncertainty in its flowrate, and in equivalence ratio, is approximately 10% at this time.

Figure 9 shows numerically-predicted peak temperature (using the Ref. 23 mechanism) vs. stretch rate for both planar and tubular methane-air flames with $\phi=0.53$. Unlike the hydrogen-air results, both types of methane-air flames have essentially the same peak temperature at any given stretch rate. There are discrepancies on the order of 20 K but there is not a significant difference between the two types of flames as for the hydrogen-air data. This is expected since the Lewis number for the lean methane-air mixtures is very close to one, as compared to the very low Lewis number of the lean hydrogen-air mixtures, and the effect of flame curvature becomes more pronounced as Lewis number departs from unity.

Planar Lean Methane-Air Flames versus Hot Products

Pollutants can be formed in very lean regions of direct injection engines, but the presence of hot products can improve combustion in these regions. In an effort to understand how the presence of hot products influences lean combustion, several planar flames have been investigated, where one of the impinging jets is a hydrogen-air mixture that has a

relatively fast flame speed and hence acts essentially as a hot products jet. Similar work has already been performed for planar propane-air flames versus hot products.^{25,26} Methane fuel is a good alternate to propane because of methane's well-known kinetics. A preliminary investigation using methane has already been performed but problems were encountered with the opposed jet burner used at the time.²⁷ Hydrogen-air flame attachment to the sintered metal plate at the nozzle exit (used to provide a top hat velocity profile) caused significant differences to exist between experimental and numerically-predicted data.

For the present work the opposed jet burner has been modified by inserting honeycomb metal "flow straighteners" into both nozzles. These inserts have 1/32 inch honeycomb cells that are 1/2 inch in length. The inserts provide a very uniform exit velocity profile for both nozzles, as verified by hot wire anemometry traverses in nonreacting flow. In addition the new honeycomb metal inserts do not cause flame attachment of either hydrogen-air or hydrocarbon-air flames. The opposed jet burner is of the design by Seshadri et al.¹⁷ which has been used extensively for hydrogen- and hydrocarbon-fueled diffusion flames and for hydrocarbon-fueled premixed flames, but now with the inserts can be used also for lean hydrogen-air premixed flames.

Experimental and numerical results of two planar flames are shown in Figs. 10 and 11. Two opposed jet flames are selected to simulate the following lean combustion situations: $\phi=0.69$ or $\phi=0.56$ premixed methane-air mixtures, with each of them impinging upon a jet of lean hydrogen-air premixed reactants ($\phi=0.28$). Since water vapor and carbon dioxide are the major products of a stoichiometric hydrocarbon reaction, it is convenient to form hot products from a lean hydrogen-air premixed flame, based on the fact that the premixed hydrogen-air flame has a fast laminar flame speed relative to the premixed hydrocarbon-air flame. Therefore the effect of stretch rate on methane flames can be studied individually, without considering the influence of stretch rate on hydrogen-air flames. Another advantage is that no carbon exists in the hydrogen-air flame products and thus, all the carbon-bearing products (i.e., carbon dioxide or carbon monoxide) come from the hydrocarbon-air premixed flames. Thus one can easily see if the hot products lead to the additional burning of the hydrocarbon fuel.

(1) Lean, "positive flame speed" methane-air flame versus hot products

Experimental measurements and numerical predictions of temperature and reactant concentrations are compared in Fig. 10 for the $\phi=0.69$ methane-air jet. As seen from the experimental data, a premixed

“positive flame speed” flame exists on the side of the stagnation plane for the methane-air mixture. Numerical data is obtained using four different chemical mechanisms: one which models hydrocarbons with only one carbon atom (C_1),²⁸ one which models hydrocarbons containing up to two carbon atoms (C_2),²⁸ GRI-Mech 3.0,²⁴ and Williams et al.²⁹ It is found that experimental profiles of all the major species and temperature match very well to the numerically predicted profiles, although the C_1 mechanism does seem to predict a weaker flame than actually exists. The agreement among predictions and experiment is very good for the remaining three mechanisms, taking into consideration experimental uncertainty.

(2) Very lean, “negative flame speed” methane-air flame versus hot products

Figure 11 shows the experimental results and numerical predictions for a lean methane-air ($\phi=0.56$) mixture impinging upon a hydrogen-air jet ($\phi=0.28$). There is only a slight difference for this situation compared to the previous “positive flame speed” flame: the methane-air equivalence ratio is dropped from 0.69 to 0.56. It is found that a lean methane-air premixed “positive flame speed” flame doesn’t exist on the methane-air side of the stagnation plane. However the methane Raman signal disappears around the stagnation plane, indicating that either the methane fuel reacts in this zone or methane is convected away at the stagnation plane. In fact, it is found there is a very weak flame that is formed by methane diffusing across the stagnation plane and reacting with the excess oxygen from the hydrogen-air premixed flame from the other jet. This weak flame is called a “negative flame speed” flame.^{30,31} This flame is so weak that it can only be seen by eye in a dark room. There are two prerequisites for this weak flame to exist: 1) high stretch rate and 2) excess oxidizer and high temperature hot products from another jet to support it. The numerically predicted results provided by the four different mechanisms are essentially the same for this negative flame speed flame, and so only the GRI-Mech 3.0 data is shown in Fig. 11.

Conclusions

Using both a tubular burner and an opposed jet planar flame burner, several hydrogen-air and methane-air flames have been examined experimentally and these data compared to numerical predictions. For hydrogen-air premixed planar flames with $\phi=0.175$, excellent agreement between experimental and numerical profiles was obtained for stretch rates up to the experimental extinction stretch rate of 185 sec^{-1} . However the numerically predicted extinction stretch rate for these planar flames is

approximately 290 sec^{-1} . For tubular hydrogen-air flames, with $\phi=0.175$ and $\kappa = 190 \text{ sec}^{-1}$, the experimental temperature profile is significantly lower than the predicted temperature profile. For the tubular hydrogen-air flames the experimental extinction stretch rate is 220 sec^{-1} , higher than the planar flame’s experimental value but far lower than the numerically-predicted extinction stretch rate of 780 sec^{-1} .

For methane-air tubular premixed flames there is good agreement between experimental and numerical extinction stretch rates for a wide range of lean equivalence ratios. However the uncertainty in the experimentally-measured equivalence ratios is approximately 10% and current work is going on aimed at reducing that uncertainty. For one particular methane-air equivalence ratio (0.53) the numerically-predicted peak temperatures for either tubular or planar premixed flames are generally the same across a wide range of stretch rates, showing curvature has little influence for these types of near-unity Lewis number flames. Planar partially-premixed flames produced by a lean methane-air jet ($\phi = 0.69$ or 0.56) opposed by a lean hydrogen-air jet ($\phi=0.28$) were examined experimentally and numerically. Excellent agreement among experimental and numerical data was obtained for both methane air equivalence ratios, and the lower one showed evidence of a negative flame speed flame where combustion occurs only by diffusion of methane across the stagnation plane into the hot products jet.

References

1. Law, C. K. (1988), “Dynamics of Stretched Flames,” *Proceedings of the Combustion Institute*, **22**, pp. 1381-1402.
2. Echehki, T., and Chen, J. H. (1996), “Unsteady Strain Rate and Curvature Effects in Turbulent Premixed Methane-Air Flames,” *Combustion and Flame*, **106**, pp. 184-202.
3. Ju, Y., Matsumi, H., Takita, K., and Masuya, G. (1999), “Combined Effects of Radiation, Flame Curvature, and Stretch on the Extinction and Bifurcations of Cylindrical CH_4 /Air Premixed Flame,” *Combustion and Flame*, **116**, pp. 580-592.
4. Smooke, M. D., and Giovangigli, V. (1990), “Extinction of Tubular Premixed Laminar Flames with Complex Chemistry,” *Proceedings of the Combustion Institute*, **23**, pp. 447-454.
5. Nishioka, M., Inagaki, K., Ishizuka, S., and Takeno, T. (1991), “Effects of Pressure on Structure and Extinction of Tubular Flame,” *Combustion and Flame*, **86**, pp. 90-100.
6. Yamamoto, K., Hirano, T., and Ishizuka, S. (1996), “Effects of Pressure Diffusion on the

- Characteristics of Tubular Flames,” *Proceedings of the Combustion Institute*, **26**, pp. 1129-1135.
7. Nishioka, M., Takeno, T., and Ishizuka, S. (1988), “Effects of Variable Density on a Tubular Flame,” *Combustion and Flame*, **73**, pp. 287-301.
 8. Libby, P., Peters, N., and Williams, F. (1989), “Cylindrical Premixed Laminar Flames,” *Combustion and Flame*, **75**, 265-280.
 9. Kitano, M., Kobayashi, H., and Otsuka, Y. (1989), “A Study of Cylindrical Premixed Flames with Heat Loss,” *Combustion & Flame*, **76**, pp. 89-105.
 10. Ishizuka, S. (1993), “Characteristics of Tubular Flames,” *Progress in Energy and Combustion Science*, **19**, pp. 197-226.
 11. Ishizuka, S. (1989), “An Experimental Study on Extinction and Stability of Tubular Flames,” *Combustion and Flame*, **75**, pp. 367-379.
 12. Yamamoto, K., Ishizuka, S., and Hirano, T. (1994), “Effects of Rotation on the Stability and Structure of Tubular Flame,” *Proceedings of the Combustion Institute*, **25**, pp. 1399-1406.
 13. Ishizuka, S. (1984), “On the Behavior of Premixed Flames in a Rotating Flow Field: Establishment of Tubular Flames,” *Proceedings of the Combustion Institute*, **20**, pp. 287-294.
 14. Ogawa, Y., Saito, N., and Liao, C. (1998), “Burner Diameter and Flammability Limit Measured by Tubular Flame Burner,” *Proceedings of the Combustion Institute*, **27**, pp. 3221-3227.
 15. Kobayashi, H., and M. Kitano, (1989), “Extinction Characteristics of a Stretched Cylindrical Premixed Flame,” *Combustion and Flame*, **76**, pp. 285-295.
 16. Kobayashi, H., and Kitano, M. (1991), “Flow Fields and Extinction of Stretched Cylindrical Premixed Flames,” *Combustion Science and Technology*, **75**, pp. 227-239.
 17. Seshadri, K., Puri, I., and Peters, N. (1985), *Combustion and Flame*, **61**, p. 237.
 18. Kim, J. S., Libby, P. A., and Williams, F. A. (1992), *Combustion Science and Tech.*, **87**, p. 1.
 19. R. J. Osborne, Skaggs, P. A., and Pitz, R. W. (1996), “Multi-Camera/Spectrometer Design for Instantaneous Line Rayleigh/Raman/LIPF Measurements in Methane/Air Flames,” AIAA 34th Aerospace Sciences Meeting, Paper No. AIAA-96-0175, Reno, Nevada, January.
 20. Kee, R. J., Rupley, F., Miller, J., Coltrin, M., Grcar, J., Meeks, E., Moffat, H., Lutz, A., Dixon-Lewis, G., Smooke, M., Warnatz, J., Evans, G., Larson, R., Mitchell, R., Petzold, L., Reynolds, L., Caracotsios, M., Stewart, W., and Glarborg, P. (1999), *User Manual*, CHEMKIN Collection III.
 21. Mosbacher, D. M., Wehrmeyer, J. A., Pitz, R. W., Sung, C. J., and Byrd, J. L. (2002), “Experimental and Numerical Investigation of Premixed Tubular Flames,” *Proc. of Comb. Institute*, **29**, in press.
 22. Mueller, M. A., Kim, T. J., Yetter, R. A., and Dryer, F., (1999), *International Journal of Chemical Kinetics*, **31**, p. 113.
 23. Kee, R. J., Grcar, J. F., Smooke, M. D., and Miller, J. A. (1985), “A Fortran Program for Modeling Steady Laminar One-Dimensional Premixed Flames.” Sandia Report 85-8240.
 24. Smith, G. P., Golden, D. M., Frenklach, M., Moriarty, N. W., Eiteneer, B., Goldenberg, M., Bowman, C. T., Hanson, R. K., Song, S., Gardiner, W. C., Jr., Lissianski, V. V., and Qin, Z. http://www.me.berkeley.edu/gri_mech/
 25. Wehrmeyer, J. A., Cheng, Z., Mosbacher, D. M., Pitz, R. W., Osborne, R. J. (2002), “Opposed Jet Flames of Lean or Rich Premixed Propane-Air Reactants versus Hot Products,” *Combustion and Flame* **128**, pp. 232-241.
 26. Cheng, Z., Wehrmeyer, J. A., and Pitz, R. W. (2002), “Opposed Jet Flames of Lean Premixed Propane-Air Reactants vs. Hot Products,” Central States Section of the Combustion Institute, Technical Meeting, Knoxville, TN, April 7-9.
 27. Cheng, Z., Wehrmeyer, J. A., and Pitz, R. W. (2002), “Opposed Jet Flames of Lean Premixed Methane-Air Reactants vs. Hot Products,” Paper AIAA 2002-4021 presented at 38th AIAA Joint Propulsion Conference, Indianapolis, IN, July 7-10.
 28. Peters, N., (1993), “Flame Calculations with Reduced Mechanisms-An Outline,” in *Reduced Kinetic Mechanisms for Applications in Combustion Systems, Lecture Notes in Physics*, N. Peters and B. Rogg (Eds.), Springer-Verlag: Berlin, Vol. M15, Ch. 1, pp 3-12.
 29. <http://maeweb.ucsd.edu/~combustion/cermech/>
 30. Sohrab, S. H., Ye, Z. Y., and Law, C. K. (1984), “An Experimental Investigation on Flame Interaction and the Existence of Negative Flame Speeds,” *Proceedings of the Combustion Institute* **20**, pp. 1957-1965.
 31. Darabiha, N., Candel, S. M., and Marble, F. E. (1986), “The Effect of Strain Rate on a Premixed Laminar Flame,” *Combustion and Flame* **64**, pp. 203-217.

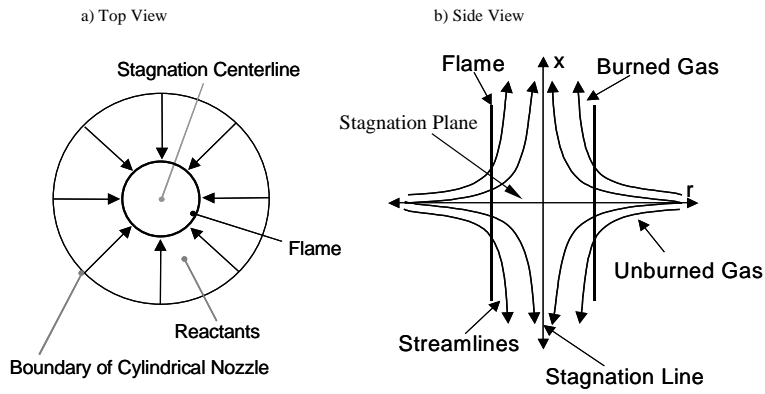


Fig. 1. Tubular premixed flame schematic.

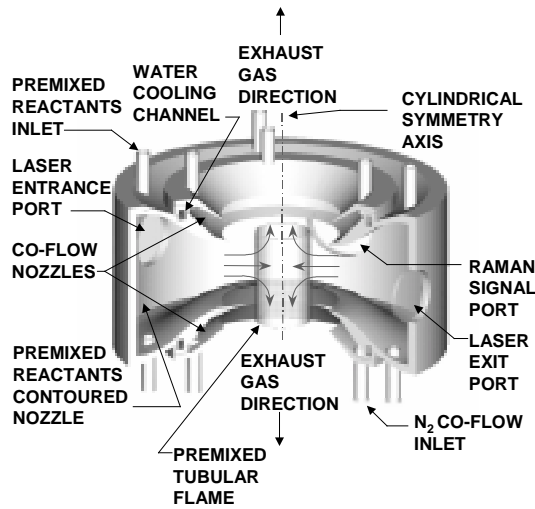


Fig. 2. Schematic of tubular burner.

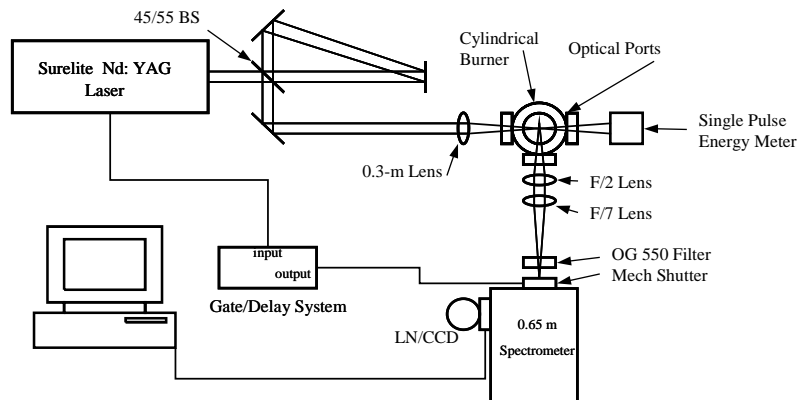


Fig. 3. Visible Raman system schematic.

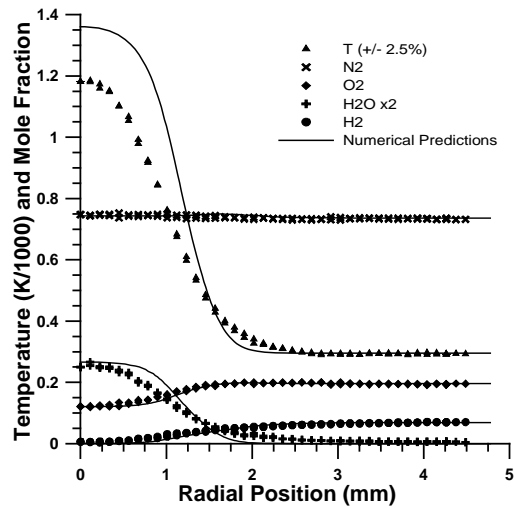


Fig. 4. Raman-derived and numerically-predicted product measurements (using Mueller et al. chemistry with thermal diffusion) in hydrogen-air tubular flame ($\phi=0.175$, $\kappa=190 \text{ s}^{-1}$).

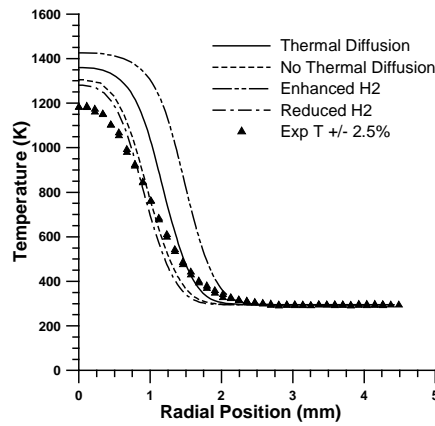


Fig. 5. Simulation (using Mueller et al. chemistry) showing effects of thermal diffusion coefficient and increasing/decreasing the binary diffusion coefficient of H_2 into N_2 by +32%/-29% in a hydrogen-air tubular flame ($\phi = 0.175$, $\kappa = 190 \text{ s}^{-1}$).

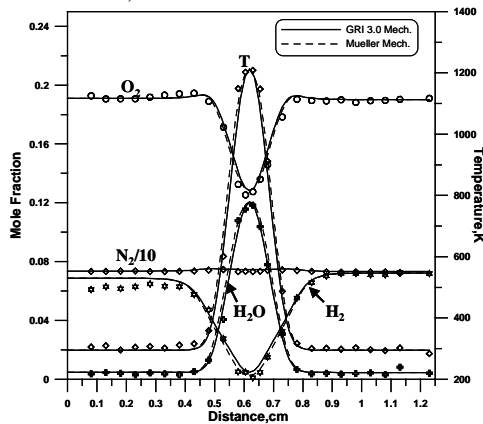


Fig. 6. Structure of planar hydrogen-air twin flame ($\phi=0.175$, $\kappa = 183 \text{ sec}^{-1}$). Numerical predictions use Mueller et al. mechanism and GRI-Mech 3.0.

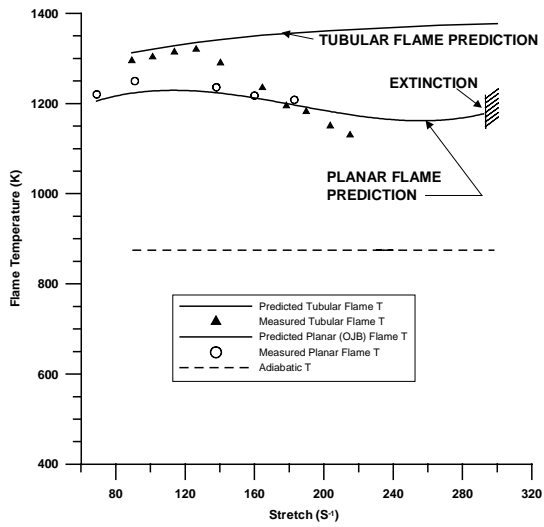


Fig. 7. Comparison of peak flame temperature vs. stretch rate for hydrogen-air tubular and planar flames ($\phi=0.175$).

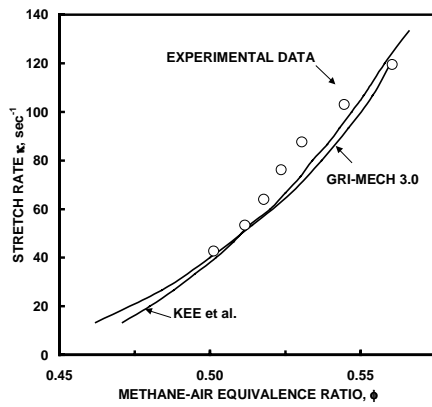


Fig. 8. Extinction stretch rate vs. equivalence ratio for premixed, tubular, methane-air flames.

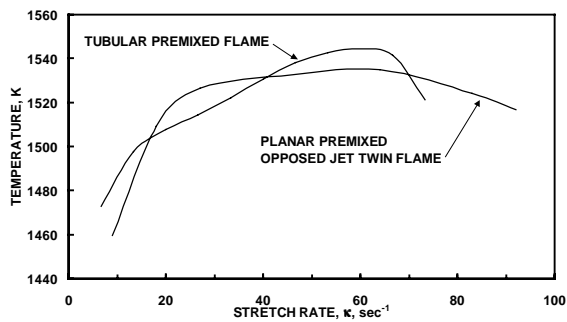


Fig. 9. Peak temperature versus stretch rate for $\phi=0.53$ methane-air premixed, tubular and planar flames.

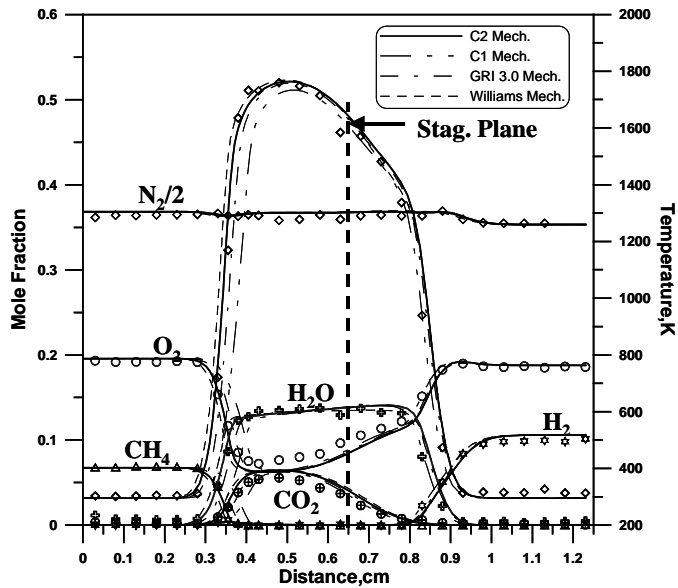


Fig. 10. Experimentally-measured and numerically-predicted structure of planar flame produced by $\phi = 0.69$ methane air jet impinging on $\phi=0.28$ hydrogen-air jet. $\kappa = 140 \text{ sec}^{-1}$. Numerical simulations shown for four different reaction mechanisms.

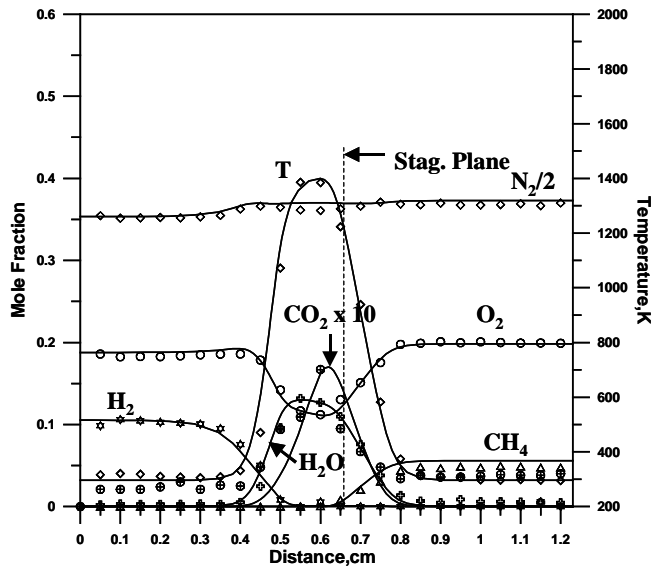


Fig. 11. Experimentally-measured and numerically-predicted structure of planar flame produced by $\phi=0.56$ methane-air jet impinging on $\phi=0.28$ hydrogen-air jet. $\kappa = 140 \text{ sec}^{-1}$. Numerical predictions obtained using GRI-Mech 3.0.